Bardi ., M.; Alejandro H. Plazas; Macian Martinez, V.; Payri Marín, R.; Ruiz Rosales, S.; Bardi, M.; Plazas, AH. (2014). Experimental study of the relationship between injection rate shape and Diesel ignition using a novel piezo-actuated direct-acting injector. Applied Energy. 118:100-113. doi:10.1016/j.apenergy.2013.12.025.

Experimental study of the relationship between injection rate shape and Diesel ignition using a novel piezo-actuated direct-acting injector

Vicente Macian [a] , Raul Payri [a] , Santiago Ruiz [a] , Michele Bardi [a] , Alejandro H. Plazas [b]

[a] CMT- Motores Térmicos, Universitat Politècnica de València, Spain

[b] GM R&D, Warren, MI, USA

Corresponding Author:

Prof. Raul Payri (rpayri@mot.upv.es)
CMT Motores Térmicos
Universitat Politècnica de València
Camino de Vera, Ed 6D, 46022
Valencia, Spain

Keywords
Rate-shaping; Direct-acting; Diesel ignition; partial needle-lift; chemiluminescence.

Abstract

Injection rate shaping is one of the most attractive alternatives to multiple injection strategies; however, its implementation has been for long time impeded by limitations in the injector technology and therefore, the experimental information available in the literature about this topic is lacking.

In this work, a novel prototype common-rail injector featuring direct control of the nozzle needle by means of a piezo-stack (*direct-acting*) allowed a fully flexible control on the nozzle needle movement and enabled the implementation of alternative injection rate shapes typologies. This state of the art injector, fitted with a 7-hole nozzle, was tested at real engine conditions studying the spatial-temporal evolution of CH* and OH* chemiluminescence intensity produced by the fuel combustion. A wide test matrix was performed in an optically accessible hot-spray test rig to understand the influence that partial needle lift and alternative injection rate shapes have on the Diesel ignition

The results showed that alternative injection rate profiles have a substantial impact on the ignition event affecting the premixed phase of the combustion and the location where the ignition takes place. Moreover, the results proved that the modifications in the internal flow caused by the partial needle lift are reflected on the ignition timing: although partial needle lift and injection pressure have similar effects on the mass flow rate, in the first case the ignition delay is reduced, while in the second the combustion is delayed as a consequence of a different spray development.

1 Introduction

Fuel-air mixing process, combustion and emission phenomena are necessarily linked together in direct injection Diesel engines [1-5]. In a scenario where the global emission standards require higher engine performances in terms of combustion efficiency and emissions reduction, all the efforts by the engine community to improve the understanding of the fuel atomization, spray development and combustion are largely justified.

Over the past decades, many studies have been carried out to develop a better understanding of the mixing process [6-8] and of the fuel ignition [9-12]. Experimental facilities, such as optically accessible engines [13] and test rig cells [11, 14] combined with imaging techniques [5, 15], have become the most common tools used in spray research. Throughout the years, the efforts put in place in these studies generated an accurate and deep understanding of the injection combustion event in Diesel engines.

On the other hand, several activities have been performed to advance the flexibility of the fuel injection system, achieving significant improvements [2]. Most of these systems are operated with electro-hydraulic actuation, where the fuel injector is activated using either a solenoid or a piezo-stack; however, the opening of the injector itself is produced by the pressure difference at the two sides of the needle limiting the injection control to an *on-off* mode. As a consequence of that, multiple injection strategies are the most employed tool to control the Diesel combustion,

although they show strong limitations in minimum dwell-time, and poor atomization during the opening/closing transient [1, 3].

The last development of piezo-actuated injectors is the so called *direct-acting* system, where a piezo actuator (stack) is mechanically coupled with the injector needle, having direct control on its position: this technologic achievement enables a fast and precise control of the fuel flow through the injector nozzle [16]. Although many researches have been oriented to the study of the injection event using conventional servo-hydraulic injectors, only a few are discussing the effect of the partial needle lift on injection process [17, 20, 21] and, to the author knowledge, none of them has been tested at real engine conditions.

In the present work, a prototype multi-hole injector featuring the direct control of the nozzle needle by a piezo-stack, has been used to investigate the effect of partial needle-lift and injection rate shaping on Diesel combustion in a wide range of conditions typical of a real Diesel engine varying rail pressure, ambient temperature and oxygen concentration.

The chemiluminescence signals emitted during the different stages of the combustion have been studied using filtered intensified cameras. In particular, the development of the cool flames has been investigated imaging the emissions of the CH* radical (filtering at 430 nm) while for the second stage ignition the attention has been focused on the OH* radical emissions (filtering at 310 nm) [10, 13, 18]. A novel optical accessible high temperature - high pressure test rig has been employed to mimic the real in-cylinder Diesel-engine thermodynamic conditions [11]. The test rig was modified in order to enable variations in ambient oxygen concentration and to simulate EGR conditions.

The combustion of the 7 spray plumes produced by the multi-hole nozzle have been imaged globally using a large visualization field (~100mm x100mm) centered on the injector nozzle, and the relationship between CH* and OH* emissions has been carefully investigated performing a simultaneous image with two synchronized ICCD cameras.

Finally, the images captured have been processed using a purpose-made Matlab routine, developed to present in a comprehensive color-maps the data related to each test and to compare the time evolution of the event under different test conditions. Finally, the combustion-related characteristics parameters (e.g. ignition delay and location) have been measured and analyzed.

2 Material and methods

2.1 Injection system

The fuel supplied to the injector is provided by a common rail system constituted by a high pressure pump and a conventional rail with a pressure regulator. The system allows fuel injections at high and relatively constant pressure (up to 200 MPa). All the injection system is electronically controlled by a ECU and all the settings are introduced digitally.

The prototype piezoelectric direct-acting injector is fitted with a 7-hole nozzle: the orifices are equally separated and oriented with 156º opening angle; the orifice outlet diameter is $D_0 = 156\,\mu m$ and $k - factor = 1.5$ [19]. All the nominal features of the injector are listed in

Table 1. In this study, the injector body temperature is controlled at 343 K [11], and commercial Diesel fuel (EU standard EN590) was used with $812\,{kg}/{m^3}$ density and $1.9\,{mm^2}/{s}$ kinematic viscosity (at 343K).

The injector used in the present work has the piezo-actuator directly coupled with the injector needle and thus, the voltage applied to the piezo-stack (in this work, also called *charge* or *Ch*) controls the needle position: the needle lift increases with the voltage applied. Since it was not possible to measure the actual needle lift, a hydraulic characterization was performed to study the relationship between mass flow rate and the voltage applied [17]. Although an important and highly-repetitive reduction in the mass flow rate is achieved by needle throttling (reducing the voltage or *charge* applied), the relationship between mass flow rate and *charge* is complex since other parameters, like injection pressure and injector temperature, are affecting the injector behavior. Therefore, in order to have a more quantitative description of the needle lift, it was preferred to use the mass flow rate and the hydraulic parameters available from [17] for the same injector. The *direct-acting* injector features also a very rapid response of the needle movement with respect to the voltage applied: this fact enables the possibility of performing *injection rate shaping*, that is, to inject fuel with variable mass flow rate (see 2.4).

The liquid- and vapor-phase penetration of the same injector have been characterized in previous works [20, 21] and it was highlighted an important relationship between needle-lift and spray spreading angle (and consequently liquid length): in particular, when the needle is throttling the fuel flow, liquid length is reduced and spreading angle is increased, as possible effects of changes in the nozzle internal flow behavior.

2.2 The facility

A novel optically accessible test chamber, capable of simulating the in-cylinder thermo-dynamic conditions of Diesel engines at the time of injection, was used. Following the convention presented in [22], the test rig is classified as a constant-pressure flow (CPF) facility: the high-pressure high-temperature gas (an adjustable mixture of atmospheric air and nitrogen depending on the specific condition tested) enters the chamber from a 30 kW electric heating system and continuously flows through the test section, obtaining typical Diesel in-cylinder conditions. Compared to other facilities [24, 28], this test rig has the unique feature of obtaining nearly quiescent and steady thermo-dynamic conditions within the chamber, providing thus high repeatability and an important reduction in the time required for the tests.

The facility is basically composed of four parts: compressors, heaters, test vessel and control system (Figure 1 left). The gas, stored by volumetric compressors in high pressure reservoirs, flows continuously through the test chamber. The temperature and pressure within the test chamber are set to the desired values respectively adjusting the power of the electrical heaters and the setpoint of the pressure regulator placed upstream of the chamber. The regulation is performed automatically by a closed loop PID system.

The test rig can work in open or close loop in order to test either with air or air/nitrogen mixtures: the chemical composition of the gas in the chamber is permanently monitored by a Horiba

system and can be adjusted adding either air or Nitrogen through a reintegration system. In this way, the recirculation of exhaust gas (EGR) can be simulated by decreasing the oxygen content of the charge in the test chamber [24].

The big total volume of the high pressure gas tanks, pipe lines and combustion chamber, guaranteed a negligible increase in H_2O content and other combustion products along the test session.

The gas-flow through the test chamber has been optimized in order to obtain the best compromise in terms of temperature homogeneity, exhaust (or fuel vapor) scavenging and spray-gas interaction (Figure 1 right). To improve the temperature homogeneity within the chamber the velocities of the gas have to be high in order to limit the wall boundary layer and maintain the whole test section at high temperature. On the other hand to study the spray in free-field-like conditions the velocities have to be low and to ease the exhaust scavenging the flow has to be organized. In Figure 1 Right a sketch of the chamber is shown: the gas inlet is a reverse-cone diffuser placed in the bottom; due to their lower density and the inertia the gas from the inlet goes toward the upper part of the chamber; then, due to the heat exchange with the surrounding walls, the gas gets cold and it is forced to move toward the only available outlets, which are placed close to the walls in the bottom of the chamber. The position of the outlets in the bottom of the chamber improves heating efficiency, since extracts the gas in a position where they are relatively colder. The complete description of the facility is provided in [11] and [20].

2.3 Methodology and optical arrangement

Chemiluminescence is a chemical phenomenon consisting in a light emission due to the decay of a molecule from an excited state to a lower energy level. OH* and CH* decay to ground state radicals have a well-defined chemiluminescence spectrum that permits identifying the emitting molecule [18, 23].

Dec and Espey [23] showed that CH* is an excellent marker for the characterization of the first phase of Diesel combustion. Its timing and location can give valuable information on Diesel cool flames development and in their experiments, CH* chemiluminescence appeared to be the fair witness of auto-ignition. The natural emission of light of the CH* radicals (432 nm) has been studied using the methodology described in [23]. The combustion process ensues with fuel breakdown following the first significant heat release and an eventual first soot formation occurring on the peak of premixed flame. This chemiluminescence lasts in rich areas of the jet during the whole combustion event but it is soon hidden by this early soot radiation that is about three orders of magnitude brighter. The methodology used in this work, proposed by Dec and Espey in [23] and followed by many other authors [11, 13] takes its stand on the acquisition of filtered images (at 430 ± 5 nm) with an intensified camera.

Studies in the literature related high-temperature Diesel reactions to the formation of OH* radicals and showed that OH* forms in nearly stoichiometric regions [9, 25]; the start of these reactions are related to the first significant heat release and, for this reason, the OH* formation

is normally studied to determine the ignition delay [9, 13]. Gaydon demonstrated that the spectrum emitted by OH* decay has an important peak at 306 nm [18]. Therefore, OH* emissions can be observed using 310 ± 5 nm interferometric filter that guarantees to exclude nearly the totality of the soot incandescence emissions dominating the spectrum at higher wavelengths, combined with an acquisition system efficient in this part of the spectrum (ICCD camera and U.V. lens) [13, 14].

To image CH* and OH* radicals' chemiluminescence two ICCD cameras have been employed simultaneously: hereafter, the cameras will be referred as *CH camera*, the camera devoted to image the CH* emission and *OH camera* the other one. The details of the configurations are described in Figure 2 and its related table.

A delay generator has been used for the camera synchronization:

- to compensate the different internal delay of the cameras, acquiring the two images simultaneously;
- to acquire images at different instants from the start of injection, performing a time sweep along the injection event (still imaging).

The time step used to increase the delay setting of the delay generator was adjusted to improve the time resolution of the tests when it was considered convenient. During the ignition phase, time steps as short as 20 μs were employed while during the diffusive flame the time steps were increased with a maximum of 200 μs. The intensifier gating time has been fixed for the two cameras at 20 μs to improve the accuracy of the data in the time domain and five test repetitions for each instant were performed to average the statistic shot-to-shot variation and to have an understanding of the precision (*repeatability*) of the tests.

The low emissions of the CH* radical together with the need of catching the very beginning of the cool flames have made light efficiency a primary issue. For this reason the two cameras were positioned to visualizing directly the combustion, avoiding the use of a beam splitter or a chromatic mirror that would reduce the light efficiency of the system. Therefore, a small angle had to be included between the camera's and the injector's axes (Figure 2) requiring a geometrical correction of the images that has been included in the image processing. In order to make sure to capture the first radical emissions, cameras' intensifiers gain were set to their maximum.

As mentioned before, after second stage ignition, soot incandescence generally leads the CH* camera sensor to saturation: being the signal acquired not related to CH* chemiluminescence anymore, the acquisition of the *CH camera* was stopped to avoid overcharging the intensifier. Due to the shorter wave length recorded by the *OH camera*, the overlap of the signal filtered and soot incandescence is limited [18] allowing to study the OH* chemiluminescence during the whole injection event.

2.4 Test matrix

The main objective of the test plan (Table 2) is to investigate the potentialities of injection rate shaping understanding its impact on the combustion event. In order to obtain reliable results, a

comparison between different injection typologies was replicated under different thermodynamic conditions typical of a real Diesel engine. For each ambient condition (oxygen content, ambient temperature and ambient density), the test was repeated modifying injection pressure, needle lift and injection rate shape.

The tests at 21% oxygen concentration were performed using atmospheric air, while exhaust gas recirculation (*EGR)* was simulated closing the gas-circuit and recirculating the gases (Figure 1); either nitrogen or air were added to the system in order to reach the desired oxygen concentration ($O_{2\%}$ = 12 – 16 %). Ambient temperature and pressure were controlled directly by a closed loop PID (see 2.2) while the ambient density was derived using Peng-Robinson equations [26].

The injected mass was fixed at 50 mg adjusting the total energizing time, in order to limit the pressure wave within the test chamber; however, injections were long enough to assure the ignition to happen before the end of the injection at all the conditions tested, excluding the effect of the closing transient from the study.

In this work, the boundary conditions will be divided in two groups: *ambient parameters,* referring to the conditions within the chamber (ambient density, ambient temperature and oxygen concentration) and *injection parameters* referring to the setting of the injection system (rail pressure, piezo-stack charge and injection rate shape).

Even if the needle lift is controlled adjusting the piezo-stack voltage (*charge*) [17], its position could not be measured experimentally and the relationship between charge applied and needle position involves also other quantities (like injection pressure and piezo-stack temperature). Therefore, the three charges tested are qualitatively referred as *low, med* and *high charge*. *High charge* corresponds to the full needle lift case, that is, when injector needle effect on fuel flow is considered to be negligible; at *med* and *low charge* the needle lift is progressively reduced, and, consequently, the related mass flow rate. A quantitative description of the different charge levels will be performed basing on the measured mass flow rate (see 4.2).

In order to understand the effect of rate shaping on *Diesel* combustion, three different injection *rate profiles* have been tested (depicted in Figure 3): *square* (conventional *top-hat* injection), *boot* and *ramp* injections. The related mass flow rate profiles were measured via Bosch method [17] and are presented in Figure 3 for two different injection pressures.

In order to avoid confusion, in this work, if not specified, the results presented are related to *square shaped* injections at *high charge*: when either the injection rate shape or the charge level is varied, it will be always indicated.

2.5 Raw images description

Figure 4 and Figure 5 present the image-sequences recorded by the two cameras for a sample test condition in order to give an overall description of the features captured in the measurements, as well as to point out the technical approach to the results analysis.

CH* emissions arise earlier and are evenly distributed in the sprays region. The shape of the area where CH* chemiluminescence is observed recalls the shape of the sprays, and, as observed by other authors, it overlaps the regions where fuel is vaporized [13, 23]. However,

the CH* intensity is very low and it is right above the camera sensor noise level. The CH* chemiluminescence intensity increases progressively up to the second stage ignition (*SSI*), when intensity suddenly rises of about three order of magnitude; afterward, it is not possible to relate the signal recorded with CH* emissions anymore, because they are disguised by broadband high temperature chemiluminescence and soot incandescence [23].

On the other hand the onset of OH* radicals shows different features: the OH* emissions start growing from separated nucleus and the intensity of the signal rises sharply and stabilizes at a certain level. The nuclei are observed at the same time and in the same areas where the *CH camera* detects the abrupt increase in the intensity confirming OH* chemiluminescence as a good marker for high temperature reactions but also the broad spectrum of the light emissions arising after the *SSI* [18]. Finally, the diffusive phase of the flame take place and the flame front stabilizes at a certain distance from the nozzle outlet (lift of length or *LOL*) [9].

The camera intensifier tends to increase its noise level when the signal intensity gets stronger: in the images presented in Figure 4 and Figure 5 the combustion causes an increment of the noise level in the entire image. The same effect is caused by the background reflections that, in the same way, falsely increase the signal in some areas of the images. This fact has to be taken into account to understand correctly the results and to avoid wrong interpretation of the data.

2.6 Data processing

Due to the number of conditions tested and the amount of information contained in each single image, it is necessary to develop a processing technique capable of condensing the information and simplifying the analysis of the results. In the following section, the approach used and the variables introduced in the data analysis are described.

2.6.1 *Contour maps*

Three-variables plots have been created by drawing contour maps on *time - radial position* axes. This graphic illustration of the results consists in the simultaneous presentation of the intensity recorded (color map) together with the radial position (*Y-axis*) and temporal data (*X-axis*), so that an entire image sequence can be presented on a single plot.

The intensity contour maps are obtained following a well-defined procedure:

- *Average filter:* in order to reduce the noise caused by the camera intensifier a mean-filter (8x8 pixels) is applied to the raw image;
- *Sectorization*: the spray-sectors are delimited (Figure 6 left) and analyzed separately;
- *Arc maximum intensity profile*: a radial intensity profile is obtained for each spray sector seeking the pixel with the highest intensity (*counts number*) at each radial position (Figure 6 right);
- *Repetition average*: the intensity profiles obtained (one per spray) are averaged over the 5 repetitions (Figure 6 right), obtaining a characteristic profile per spray per time step;

- *Spray average*: the Intensity profiles obtained by the different sprays are averaged and one characteristic average intensity profile is obtained for each time step (*Max. Arc. Int.*).
- *Contour map*: the *Max. Arc. Int.* obtained for each time step are put together in a single contour map indicating in color the final average radial intensity, on *X-axis* time after the start of the injection (*ASOI*) and Y-axis the radial position (Figure 7).

Due to the time-costing image acquisition method, the images are acquired starting right before the ignition until the end of injection: the time domain of the acquisition period is represented on the contour maps by vertical black lines (Figure 7).

2.6.2 *SoCH, SoCH* and OH_{peak}

The first- and the second-stage ignition have been defined basing on the appearance of respectively CH* and OH* radicals. Due to the very low intensity of the CH* chemiluminescence, the fisrt-stage ignition, named in this work *start of* CH* or *SoCH* has been defined as the first instant at which the signal recorded is above the sensor noise level. On the other hand, the start of OH* signal *(SoOH*) has been defined following the observations by Lillo et al. [27] and the guidelines from the Engine Combustion Network (ECN) [28]. *SoOH* is representative of the second-stage ignition and it corresponds to the parameter that in other studies is indicated as *ignition delay* [11, 13].

A criterion based on the intensity time evolution during the combustion is adopted: in Figure 8 the parameter *Max. Int.* (that is the maximum of the *Max. Arc. Int.* for each instant) obtained for all the tests performed are presented on the same plot: the *time-axis* for each case is shifted arbitrarily in order separate the different groups. The plot shows clearly that the curves are always characterized by a steep increase followed by a peak and then, a nearly-steady period. Even if oxygen concentration is the main driver for the value of this peak in OH* chemiluminescence intensity (OH_{peak}), other authors showed that it is related also to other boundary conditions and it is representative of the premixed phase of the Diesel combustion [29].

In order to obtain coherent results, the differences in peak intensity observed have been taken into account calculating a specific threshold for each test condition and using as reference the intensity at the peak OH_{peak}. Finally, the threshold used for *SoOH* calculation, ths_{OH} is defined as

$$ths_{OH} = \frac{OH_{peak}}{2} \tag{1}$$

Summarizing, for a datum test condition the following definitions are given:

- First-stage ignition delay (*SoCH*): instant at which the first detectable CH* chemiluminescence signal is recorded;
- OH_{peak}: OH* chemiluminescence intensity peak value reached right after the *OH** signal appearance;

- Second-stage ignition delay (*SoOH*): instant at which the variable *Max. Int.* exceeds ths_{OH};
- M_{OH}: the fuel mass injected before the *SoOH* and thus a central parameter for the premixed phase of the combustion. This parameter is derived crossing the data from mass flow rate measurement and *SoOH*.

Moreover the radial distance corresponding to the OH_{peak} has been determined to complete the information of the ignition event.

3 Results

The results' session is divided into two main parts: the first, presenting the relationship between the ignition event and the *ambient parameters*, and the second studying the effect of the *injection parameters* with special focus on the unique features of the *direct-acting* injector and evaluating its capabilities of controlling the fuel ignition.

3.1 Effect of ambient conditions

As described earlier, the images obtained in the tests have been re-elaborated and condensed into maps relating the intensity of the radiation obtained in the images with the time *ASOI* and its radial position. Liquid and vapor phase penetration data of the tested injector are available from previous test campaigns [20, 21] and are plotted on the contour maps: these data are a valuable reference for a global understanding of the results. The test matrix studied in liquid and vapor phase measurement campaigns is identical to the one tested in this work except for temperature and ambient gas composition:

- the tests were performed at T_{amb} = 870 and 950 K (in this study T_{amb} = 870 and 935 K); therefore, the cases tested in this work at T_{amb} = 935 K will be compared to the data of the former experiments at T_{amb} = 950 K being the most similar temperature.
- the injection were performed in nitrogen atmosphere in order to prevent the combustion;

However, the bias introduced in the data by the differences mentioned above is considered negligible, especially for the purpose of this comparison.

In Figure 9, CH* and OH* chemiluminescence contour-maps obtained at different oxygen concentration are presented. The differences between the CH* and OH* chemiluminescence onset described in section 2.5 is confirmed: CH* emissions appears smoothly (note the color scale on the left) and distributed over a wide region starting close to the spray tip. Even if the background reflections combined with the intensifier noise (see 2.5) avoids an accurate detection of the boundaries of the chemiluminescence emission region, the map highlights a relationship between the CH* emissions and the region included between the vapor and the liquid phase penetration; on the other hand, the OH* chemiluminescence appears later, and the transition of the signal intensity from its appearance to its maximum is faster. Ambient oxygen contempt has a different impact on the OH* and CH* development: reminding that CH* measurement can be related to this radical only before the onset of high temperature reactions

(OH* apparition), the timing and the position of its detection is barely affected by the oxygen concentration; differently, passing from 12 to 21% oxygen concentration causes a faster apparition of the OH* radicals and moves the reaction region closer to the nozzle tip; Moreover a higher oxygen concentration causes an important increase in the OH* chemiluminescence intensity.

Figure 10 shows the impact of the ambient temperature on the measured variables. As in the previous case CH* chemiluminescence appears close to the spray tip, while OH* signal appears well behind the vapor penetration boundary. A reduction in the ambient temperature delays the apparition of OH* radicals but in this case (differently from the effect of oxygen concentration) the CH* chemiluminescence apparition is delayed in a similar way. No significant changes are observed in the intensity of both chemiluminescence signals. The color-maps presented in Figure 10 show also another important feature: right after its first apparition the OH* chemiluminescence shows a local maximum in the intensity. This feature observed also by other authors [10, 11] is related to the premixed phase of combustion: the location and the magnitude of this local maximum in the next sections will be related to the test conditions.

3.2 Effect of injection parameters

The dependence of the ignition process on the *injection parameters* has been studied focusing on two points:

- the comparison of the effect of a reduction in mass flow rate due to a reduction in p_{rail} and a reduction in mass flow rate due to the partial needle lift (needle throttling);
- the effect of a modification of the mass flow rate in the first part of the injection fixing the final mass flow rate performing *rate shaping*.

In the first comparison, a reduction in mass flow rate from a reference test condition (p_{rail} = 150 MPa, *ch* = high, Figure 11-top) has been obtained in two different ways: the first reducing the injection pressure, maintaining the maximum needle lift (p_{rail} = 60 MPa, *ch* = high, Figure 11-middle) and the second reducing the needle lift but maintaining the injection pressure (p_{rail} = 150 MPa, *ch* = low, Figure 11-bottom). The comparison shows that the main effect on the measured variables of a decrease in mass flow rate is reduction of the radial position of the emissions. The CH* emissions, as discussed before, are strongly related to the spray penetration, that depends on spray momentum and then mass flow rate [30, 31]. However, the radial position of the first CH* detection is similar in the three cases compared, while the first OH* detection moves farther from the nozzle tip when the mass flow rate is increased. The gas-jet theory [32, 33] can offer a path to understand this phenomenon: following this interpretation of the diesel spray a modification in the mass flow rate does not affect the spatial domain of the mixing field, but it only contracts or dilates the time scale; in other words, even changing the mass flow rate, at a datum spray penetration the mixing field is identical (this is true if the spreading angle is not changing, but at this degree of approximation, it can be considered constant). The fact that the CH* radicals location is not affected by injection parameters links this measurement to the mixing field. On the other hand, OH* chemiluminescence has to be

intended as the final stage of the pre-reactions: the time needed for the pre-reactions to be completed mainly depends on the chemical/physical condition of the mixture: this lapse of time, approximately constant for the different injection cases shown in Figure 11, causes a farther location of the ignition location for spray penetrating faster (at higher mass flow rate).

In the following comparison the injection rate shape has been modified changing the mass flow rate during the first part of the injection but reaching the same level during the final stage. The related injection rate profiles have been presented in Figure 3. Apart of the modification in the liquid and vapor phase penetration associated with the injection rate shaping and already described in [20, 21] the main differences caused by the alternative injection rate shapes concern the location and the intensity of the peak in the OH* emissions observed at the ignition (see Figure 12).

Therefore, this feature on the contour map suggests that injection rate shaping affects the premixed phase of the combustion: this phase is very important because it is responsible for the peak in the rate of heat release normally observed at the ignition that causes the typical Diesel engine noise problems, and the formation of NO_x [3, 4]. The reduction of the intensity peak observed is an encouraging insight of the effectiveness of these injection strategies.

In the next section the data showed in the color maps will be summarized in some key parameters, enabling the presentation of a global picture of the results.

4 Discussion

The results presented in the previous section helped understanding the details of the modifications taking place in the ignition process when a single test condition was modified. However, the contour-maps are effective to compare only a limited number of cases. In this section, the parameters describing the salient features of the contour maps are presented in order to observe the global trends of the results. Due to the huge amount of information gathered in the tests this section will focus only on the most significant parameters obtained.

4.1 Effect of ambient parameters

The first parameters of interest are *SoCH* and *SoOH* which, as previously discussed, are representative of the time at which, respectively, first- and second-stage ignition begin. The plots presented in Figure 13 show and relate with them the effect that $O_{2\%}$, T_{amb}, and *BP* fixing the *injection parameters*. The comparison confirms and extends the observations done before:

- an increase in ambient temperature and backpressure causes an increase equally in *SoCH* and as in *SoOH*;
- oxygen concentration affects mainly *SoOH* while it has a only second order effect on *SoCH.*

The dwell time between *SoCH* and *SoOH* in Figure 14 is coherent with the previous observations but offers a different point of view: $O_{2\%}$ and *BP* are the main drivers for this parameter while a variation in ambient temperature appears to have only a second order effect. These observations are deeply related with the physical and chemical processes taking place in

the Diesel spray and are in accordance with what found in other works [10, 29]. The results presented achieve two goals: i) confirms what found in other works adding new information related to the specific conditions tested; ii) proves the reliability of the techniques employed and gives a further support to the evaluation of the direct-acting injector capabilities, that is the main objective of the present work.

4.2 Effect of injection parameters

In this section, the most important findings of this work concerning the effect of injection parameters on the ignition process are presented.

In order to compensate the lack of quantitative information about the needle lift, following the approach used in [20], the non-dimensional parameter λ has been introduced to quantify the throttling effect of the needle:

$$\lambda = \frac{\dot{m}}{\dot{m}_{f.n.l.}} \tag{2}$$

where $\dot{m}$ is the average mass flow rate for a specific charge level and $\dot{m}_{f.n.l.}$ is the average mass flow rate at same injection pressure but at full needle lift (*high* charge level). For the *boot* shaped injection the same parameter has been similarly defined as

$$\lambda = \frac{\dot{m}_{foot}}{\dot{m}_{f.n.l.}} \tag{3}$$

where $\dot{m}_{foot}$ is the average mass flow rate during the first part of a *boot* shaped injection, the so called *foot.*

This parameter is used to compare the conventional injections at different charge levels together with the *boot* type injection considering that in most of the cases ignition delays are lower than 1 ms, that means that the ignition is related only to the *foot* part of the injection; the results related to the *ramp* shaped injection, will be included on the same plot for reference, with an indication on the *x-axis*.

The effect of injection parameter on *SoOH* (Figure 13) is limited, and the variations observed fall within the limit of the experimental accuracy. However, in the conventional *square* injections some slight trends can be captured:

- injection pressure tends to reduce the *SoOH* due to his enhancing effect on the mixing process; this effect has already been observed in other works [23, 29, 34];
- the needle fuel throttling shows a small effect in reducing the *SoOH*.

Even if this second effect is small, it is interesting to underline that this effect can be explained only assuming that reducing the needle lift the spray development is modified. In fact, if the spray development at the different needle lifts was the same, the effect of the fuel throttling should be similar to the effect of a reduction in the injection pressure and therefore the *SoOH* should be longer at lower values of λ. However, the trend observed is the opposite. This fact can be explained by the observations presented in the previous studies carried out on this injector [17, 20, 21]: in this works it has been observed that the fuel throttling operated by the

nozzle needle has consequences on the fuel flow through the orifices that are eventually reflected on the spray development as an increase of the spray spreading angle. Indeed, the increase in the spreading angle enhances the mixing process and it is in accordance to the reduction in the *SoOH* observed.

Another interesting feature appearing in the contour maps is the peak in the intensity that has been observed right after the second stage ignition. As mentioned in section 3.1, this characteristic is linked to the premixed phase of the Diesel combustion and injection parameters that control the amount ignitable mixture formed at the moment of the ignition. The measurement of the OH_{peak} is meaningful only in the case that the premixed combustion takes place entirely in the field of view: analyzing the images of the tests it has been observed that for some combination of test conditions (e.g. T_{amb} = 870 K and p_{rail} =150 MPa) the premixed combustion was partially out of the field of view, and the results related to these tests were not reliable. For this reason they have not been included in the plot below.

The results in Figure 16 confirmed that a reduction in the mass flow rate (either by reducing the injection pressure or by partial needle lift) causes a reduction in OH_{peak}. Moreover, it is important to observe that for all the ambient conditions presented in the plot, the lowest OH_{peak} is achieved using the non-conventional injection rate shapes (*boot* and *ramp*). Therefore, profiling the mass flow rate reducing the fuel flow before the ignition has interesting consequences on the ignition event. This observation is also sustained by the calculation of the mass injected at the moment of the ignition ($M_{ignition}$): this parameter, obtained comparing the *SoOH* with the mass flow rate measurements performed in [17], shows the same behavior of OH_{peak} and therefore confirms the relationship between OH_{peak} and the premixed combustion (Figure 17).

Summarizing, the analysis of *SoOH*, OH_{peak} and $M_{ignition}$ reveals that none of the injection parameters has substantial effects on the ignition timing (SoOH); on the other hand, the analysis of OH_{peak} and $M_{ignition}$ suggests that the introduction of injection rate shaping helps reducing the amount of heat released during the premixed phase; many studies showed that reducing the fuel burnt during this phase of the combustion brings benefits in terms of reduction of the combustion noise and NO_x production [2, 3].

Another fundamental measurement when evaluating the Diesel ignition is the radial location where the ignition takes place: in fact, in a real engine the location of the ignition can determine radical changes in the thermodynamic conditions of the mixture, especially when it occurs in the proximity of the piston bowl. In this case, even if the fuel sprays are injected in free field conditions (the test chamber is big compared to the spray), this parameter helps investigating the combustion-control capabilities of these injection typologies. The radial distance of the ignition location increases with the mass flow rate: either a decrease in injection pressure or in piezo-stack charge causes the fuel to ignite closer to the injector tip; however, the most significant impact on the ignition location is achieved with the alternative injection rate profile, allowing a substantial reduction in the radial ignition location without modifying neither the injection pressure nor the mass flow rate at the end of the injection. This fact is particularly important for the typical low load engine conditions (i.e. low ambient

density/temperature/oxygen content) where ignition takes place far from the injection nozzle and the interaction with the piston bowl becomes an issue (i.e. wall impingement, quenching). Again, injection rate shaping showed promising results as regards as capabilities in the control of the combustion event.

As commented for the previous graphics, modifying either the injection pressure or the needle lift has similar effect on the mass flow rate, and this effect is evenly reflected on the OH_{peak} and its location. However, it has been demonstrated [20, 21] that the fuel throttling operated when the needle lift is reduced (low values of λ), the spray development is modified enhancing the mixing process. *SoOH* results confirmed these observations even if the differences observed fall in the range of the measurement uncertainties. Figure 19 compares the $M_{ignition}$ and OH_{peak} radial position data, basing on the average mass flow rate. In this way, the effect of the injection pressure and of the needle lift can be compared directly. The plots show that the driving parameter for these magnitudes is the average mass flow rate; however, at a closer look, the points at partial needle lift (*low* and *med* piezo-stack charge) are not aligned to the line connecting the points at full needle lift (dashed lines in Figure 19): this fact remarks that reducing the mass flow rate either by lowering the injection pressure or by needle throttling has a different impact on the ignition, as a consequence of differences in the spray development.

5 Summary and Conclusions

For the first time, the relationship between injection rate shape and diesel ignition has been studied experimentally. This work has been carried out using a novel piezo-actuated direct-acting injector prototype and imaging the CH*/OH* chemiluminescence under a wide range of test conditions.

The test plan carried out allowed a characterization of the first- and second-stage ignition under a wide range of test conditions, assessing the impact of the different parametric variations:

- the timing of the first- and second-stage ignition is strongly dependent on the ambient conditions;
- the fisrt-stage ignition timing mainly depends on the mixture temperature and therefore only on ambient temperature and ambient density, while the duration of the transition to the second-stage ignition is driven primarily by the chemistry of the mixture involving therefore also the oxygen concentration.
- the partial needle lift causes a slight shortening of the second-stage ignition delay (*SoOH*) as a consequence of the modifications of the increase in the spray spreading angle observed for these conditions [20];
- non-conventional injection rate profiles (*boot* and *ramp)* have a significant impact on the premixed phase of the combustion (reducing OH_{peak} and M_{OH}) and on the ignition location (reducing the radial position of the ignition) without varying neither the injection pressure nor the final fuel mass flow rate.

As a consequence of that the direct acting injector is particularly attractive from the engine point of view:

- the alternative injection rate profiles improve significantly the control on the combustion event and the flexibility of the injection system since the mass flow rate is not dependent anymore on injection pressure, and therefore the injection conditions can be changed instantaneously from one cycle to the following one;
- a valuable alternative to multiple injection strategies is available to control the premixed phase of the combustion which is among the main causes for combustion noise and the NO_x production;
- the possibility of controlling the ignition location maintaining constant the final mass flow rate (e.g. performing *boot* or *ramp* shaped injections), is very useful at low-load engine conditions: at these working points (typically at low ambient temperature/density and oxygen content) the ignition location moves farther from the injector nozzle, making of wall impingement and flame quenching an issue.

Acknowledgment

This work was sponsored by General Motors R&D, Warren, MI. The authors would like to thank Jose Enrique del Rey, Moises Ferrandez Hermosilla and Juan Pablo Viera for their precious help in the laboratory during the tests.

Bibliography

[1] Han PS, Hyun YS, Sik LC. Effects of multiple-injection strategies on overall spray behavior, combustion, and emissions reduction characteristics of biodiesel fuel. Applied Energy 2011;88:88-98.
[2] Catania AE, Ferrari A. Development and performance assessment of the new-generation CF fuel injection system for diesel passenger cars. Applied Energy 2012;91:483-95.
[3] Dober G, Tullis S, Greeves G, Milovanovic N, Hardy M, Zuelch S. The impact of injection strategies on emissions reduction and power output of future diesel engines. SAE International 2008;2008-01-0941.
[4] Rollbusch C. Effects of hydraulic nozzle flow rate and high injection pressure on mixture formation, combustion and emissions on a single-cylinder DI light-duty diesel engine. International Journal of Engine Research 2011;13:323-39.
[5] Mosburger M, Sick V, Drake MC. Quantitative high-speed imaging of burned gas temperature and equivalence ratio in internal combustion engines using alkali metal fluorescence. International Journal of Engine Research 2013.
[6] Pickett LM, Manin J, Genzale CL, Siebers DL, Musculus MPB, Idicheria CA. Relationship Between Diesel Fuel Spray Vapor Penetration/Dispersion and Local Fuel Mixture Fraction. SAE International Journal of Engines 2011;4:764-99.
[7] Bruneaux G. Development of optical diagnostic techniques to correlate mixing and auto-ignition processes in high pressure Diesel jets. Oil & Gas Science and Technology-Revue de l'IFP 2008;63:461-77.
[8] Zhu J, Kuti OA, Nishida K. An investigation of the effects of fuel injection pressure, ambient gas density and nozzle hole diameter on surrounding gas flow of a single Diesel spray by laer-induced fluorescence-particle image velocimetry technique. International Journal of Engine Research 2012.
[9] Dec JE. A conceptual model of DI diesel combustion based on laser-sheet imaging. Warrendale, PA: Society of Automotive Engineers 1997.
[10] Higgins B, Siebers D, Aradi A. Diesel-Spray ignition and premixed-burn behavior. SAE International 2000;2000-01-0940.
[11] Payri R, García-Oliver JM, Bardi M, Manin J. Fuel temperature influence on Diesel sprays in inert and reacting conditions. Applied Thermal Engineering 2012;35:185-95.
[12] Zigan L, Shi J-M, Krotow I, Schmitz I, Wensing M, Leipertz A. Fuel property and fuel temperature effects on internal nozzle flow, atomization and cyclic spray fluctuations of a direct injection spark ignition–injector. International Journal of Engine Research 2013.
[13] Payri R, Salvador FJ, Gimeno J, De la Morena J. Effects of nozzle geometry on direct injection diesel engine combustion process. Applied Thermal Engineering 2009;29:2051-60.
[14] Pickett LM, Genzale C, Bruneaux G, Malbec L-M, Hermant L, Christiansen C, et al. Comparison of Diesel spray combustion in different high-temperature, high pressure, facilities. SAE international 2010;2010-05-01.
[15] Hampai D, Marchitto L, Dabagov SB, Allocca L, Alfuso S, Innocenti L. Desktop X-ray Tomography for Low Contrast Samples. Nuclear Instruments and Methods in Physics Research Section B: Beam Interactions with Materials and Atoms 2013;309: 264-267.
[16] Kastner O, Atzler F, Juvenelle C, Rotondi R, Weigand A. Directly actuated piezo injector for advanced injection strategies towards cleaner diesel engines. 7th Int symposium towards cleaner diesel engine TDCE2009.
[17] Payri R, Gimeno J, Venegas O, Plazas A. Effect of partial needle lift on the nozzle flow in Diesel fuel injectors. SAE Technical Paper 2011;2011-01-1827.
[18] Gaydon AG. The spectroscopy of flames. London: Chapman & Hall 1957.
[19] Macián V, Bermúdez V, Payri R, Gimeno J. New technique for determination of internal geometry of a diesel nozzle with the use of silicone methodology. Experimental Techniques 2003;27:39-43.
[20] Payri R, Gimeno J, Bardi M, Plazas AH. Study liquid length penetration results obtained with a direct acting piezo electric injector. Applied Energy 2013;106:152–62.
[21] Payri R, Gimeno J, Viera JP, Plazas AH. Needle lift profile influence on the vapor phase penetration for a prototype diesel direct acting piezoelectric injector Fuel 2013;113:257-65.
[22] Baert RSG, Frijters PJM, Somers B, Luijten CCM, de Boer W. Design and operation of a high pressure, high temperature cell for HD diesel spray diagnostics: guidelines and results. SAE paper 2009;2009-01-0649.

[23] Dec JE, Espey C. Chemiluminescence imaging of autoignition in a DI diesel engine. SAE International 1998;982685.
[24] Meijer M, Somers LMT, Johnson J, Lee SY, Malbec L-M, Bruneaux G, et al. Engine Combustion Network (ECN): characterization and comparison of boundary conditions for different combustion vessels. Atomization and Sprays 2012;22:777-806.
[25] Dec JE, Coy EB. OH radical imaging in a DI diesel engine and the structure of the early diffusion flame. SAE International 1996;960831.
[26] Peng, DY, Robinson, DBA. new two-constant equation of state. Industrial & Engineering Chemistry Fundamentals, 1976;15:59-64.
[27] Lillo PM, Pickett LM, Persson H, Andersson O, Kook S. Diesel spray ignition detection and spatial/temporal correction. SAE International Journal of Engines 2012;5:1330-46.
[28] Bardi M, Payri R, Malbec L-M, Bruneaux G, Pickett LM, Manin J, et al. Engine combustion network: comparison of spray development, vaporization and combustion in different combustion vessels. Atomization and Sprays 2012;22:807-42.
[29] Benajes J, Payri R, Bardi M, Martí-Aldaraví P. Experimental characterization of diesel ignition and lift-off length using a single-hole ECN injector. Applied Thermal Engineering 2013;58:554-63.
[30] Naber JD, Siebers DL. Effects of gas density and vaporization on penetration and dispersion of diesel sprays. SAE paper 1996;960034.
[31] Desantes JM, Pastor JV, Payri R, Pastor JM. Experimental characterization of internal nozzle flow and diesel spray behavior. part ii: Evaporative conditions. Atomization and Sprays 2005;15:517-43.
[32] Musculus MPB, Kattke K. Entrainment waves in diesel jets. SAE International Journal of Engines 2009;2:1170-93.
[33] Pastor JV, López JJ, García JM, Pastor JM. A 1D model for the description of mixing-controlled inert diesel sprays. Fuel 2008;87:2871-85.
[34] Payri R, Salvador FJ, Gimeno J, De la Morena J. Influence of injector technology on injection and combustion development-Part 2: Combustion analysis. Applied Energy 2011;88:1130-9.

Notation

Symbol	Description	Units
ASOI	After the start of the injection	[μs]
BP	Back pressure	[MPa]
Ch	Voltage level applied to the piezo-stack (*charge*)	[-]
CPF	Constant Pressure Flow	[-]
D_0	Nominal diameter	[μm]
ECN	Engine Combustion Network	[-]
EGR	Exhaust gas recirculation	[-]
k-factor	Nozzle orifice conicity factor, defined as $k-factor = 100\frac{D_i - D_0}{L}$	[-]
ICCD	Intensified CCD sensor	[-]
LOL	Lift-off length	[mm]
$M_{ignition}$	Fuel mass injected at the moment of second stage ignition	[mg]
$O_{2\%}$	Oxygen content (vol.)	[%]
OH_{peak}	OH* chemiluminescence intensity peak (see 2.6.2)	[a.u]
P_{rail}	Injection pressure	[MPa]
SoCH	First-stage ignition delay	[μs]
SoOH	Second-stage ignition delay	[μs]
SSI	Second stage ignition	[-]
T_{amb}	Ambient temperature	[K]
ths_{OH}	Intensity Threshold for ignition delay (see 2.6.2)	[-]
λ	Parameter defined in 4.2	[-]
λ_{foot}	Parameter defined in 4.2	[-]
ρ_{amb}	Ambient density	[kg m^{-3}]
$\dot{m}$	Average mass flow rate	[g s^{-1}]
$\dot{m}_{f.n.l.}$	Average mass flow rate at full needle lift	[g s^{-1}]
$\dot{m}_{foot}$	Average mass flow rate at the first part of a boot shaped injection	[g s^{-1}]

List of Tables

Table 1: Injector features

Injector features	
Brand	Continental
Nozzle seat type	micro-sac
Number of orifices	7
Spray included angle	156º
Outlet diameter	0.156 mm
*k - factor**	1.5
Discharge coefficient	0.81

**k-factor definition is defined in [19]*

Table 2: Test matrix.

Parameters	Values	Unit
Fuel	Commercial Diesel	-
Injected fuel mass	50	mg
Coolant temperature [T_f]	343	K
Gas pressure [*BP*]	2.0 - 3.5 - 5.0 - 6.5	MPa
Gas temperature [T_{amb}]	870 - 935	K
Injection pressure [p_{rail}]	60 - 150	MPa
Piezo-stack charge [*Ch*]	low - med -high	-
Injection rate shape	square - boot - ramp	-
O_2 concentration [$O_{2\%}$]	12 - 16 - 21	% (vol.)

List of Figure Captions

Figure 1: Test rig. Left: Global scheme of the facility. Right: scheme of the test chamber. The gas inlet and outlet together with the injector position are indicated.

Figure 2: Optical arrangement. Scheme and details of the optical set-up and the synchronization system.

Figure 3. Injection rate shape typologies. Mass flow rate measurement for different injection rate *shapes*: *square (ch = high), boot* and *ramp* type injections at p_{rail} = 60 MPa (left) and p_{rail} = 150 MPa (right).

Figure 4: CH* and OH* formation. Time-sequence of images captured simultaneously by the two intensified cameras. $O_{2\%}$ = 16%, T_{amb} = 935K, *BP* = 5 MPa, p_{rail} = 60 MPa, *Ch* = *high*. The injector nozzle is indicated with a white spot.

Figure 5: CH* and OH* formation. Time-sequence of images captured simultaneously by the two intensified cameras. Square, $O_{2\%}$ = 16%, p_{rail} = 60 MPa, T_{amb}= 935K, *Ch* = high. The injector nozzle is indicated by a white spot.

Figure 6: Steps to obtain the contour maps. Sectors delimitation (left) and *Max. Arc. Int*. for the sector indicated by the arrow (right). The light color lines represent the single-shot profiles while the solid lines indicate the average over the repetitions.

Figure 7: Steps to obtain the contour maps. Comparison between contour maps and raw images. The vertical black lines on the contour map represent the start and the end of the camera acquisition period.

Figure 8: OH* Max. Int. versus time for the different conditions tested. Each line corresponds to a different test condition. Different oxygen concentration and temperature are shifted on the x-axis to separate the different groups and show the different behaviors.

Figure 9: Effect of oxygen concentration. Contours maps for CH* (left) and OH* (right) chemiluminescence emissions at different oxygen concentration. The related liquid- and vapor-phase penetration are indicated respectively by the dashed and solid lines. T_{amb} = 935 K, *BP* = 5 MPa, p_{rail} = 60 MPa, *Ch* = high.

Figure 10: Effect of T_{amb}. Contours maps for CH* (left) and OH* (right) chemiluminescence emissions at different ambient temperatures. The related liquid- and vapor-phase penetration are indicated respectively by the dashed and solid lines. $O_{2\%}$ = 16%, *BP* = 5 MPa, p_{rail} = 60 MPa, *Ch* = high.

Figure 11: Effect of p_{rail} and *Ch*. Contours maps for CH* (left) and OH* (right) chemiluminescence emissions at different injection conditions. The related liquid- and vapor-phase penetration are indicated respectively by the dashed and solid lines. $O_{2\%}$ = 16%, T_{amb} = 935 K, *BP* = 5 MPa.

Figure 12: Effect of injection rate shape. Contours maps for CH* (left) and OH* (right) chemiluminescence emissions at different injection conditions. The related liquid- and vapor-phase penetration are indicated respectively by the dashed and solid lines. $O_{2\%}$ = 16%, T_{amb} = 935 K, *BP* = 5 MPa, p_{rail} = 60 MPa.

Figure 13: *SoCH* and *SoOH* at different test conditions. On the left plot the data are plotted versus ambient temperature at fixed back pressure (*BP* = 5 MPa) while in the right plot the ambient temperature and the oxygen content are fixed ($O_{2\%}$ = 21%, T_{amb} = 935 K). In all the cases the same injection has been tested: p_{rail} = 60 MPa, *ch = high*.

Figure 14: *SoCH* / *SoOH* dwell time at different test conditions. On the left plot the data are plotted versus ambient temperature at fixed back pressure (*BP* = 5 MPa) while in the right plot the ambient

temperature and the oxygen content are fixed ($O_{2\%}$ = 21%, T_{amb} = 935 K). In all the cases the same injection parameters have been kept: p_{rail} = 60 MPa, *ch* = *high*.

Figure 15: *SoOH* at different test conditions. Each plot presents the effect of the injection parameters at different ambient conditions. *BP* = 5 MPa.

Figure 16: OH_{peak} at different test conditions. Each plot presents the effect of the injection parameters at different ambient conditions. *BP* = 5 MPa.

Figure 17: $M_{ignition}$ at different test conditions. Each plot presents the effect of the injection parameters at different ambient conditions. *BP* = 5 MPa.

Figure 18: OH_{peak} axial location at different test conditions. Each plot presents the effect of the injection parameters at different ambient conditions. *BP* = 5 MPa.

Figure 19: $M_{ignition}$ (left) and OH_{peak} radial position (right) at different test conditions. On the left plot the value at $O_{2\%}$=21% have been scaled to ease comparison of the results; the dashed lines connect the results related to the tests at full needle lift. *BP* = 5 MPa, T_{amb} = 935 K.

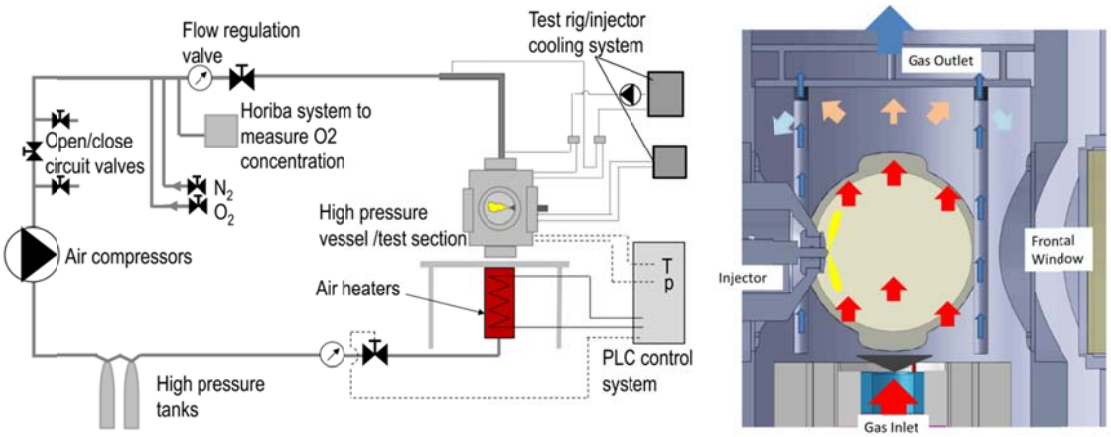

Figure 1

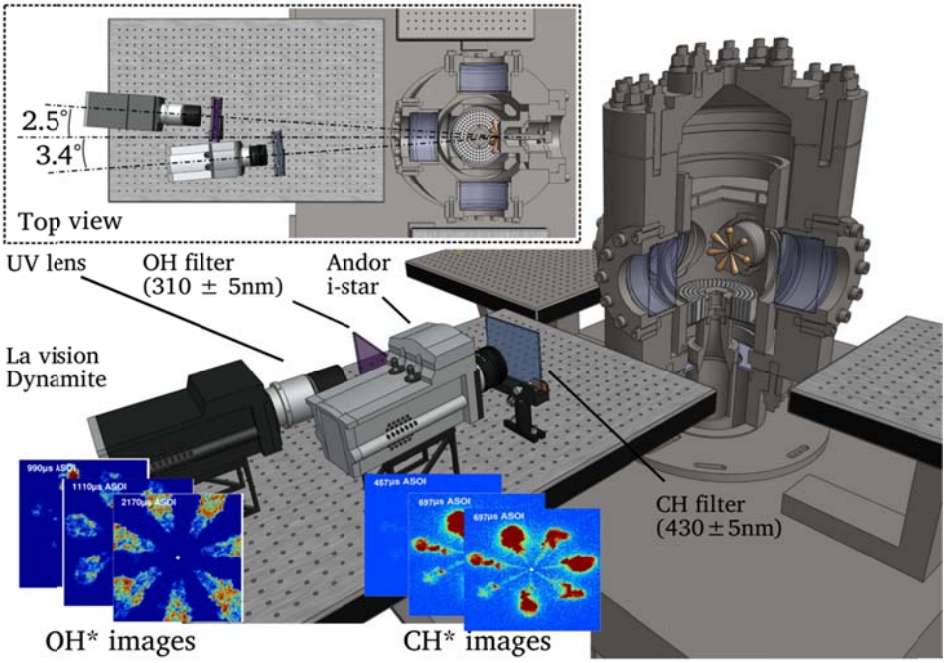

	*CH**	*OH**
Camera	Andor - Istar	La Vision - Dynamight
Sensor type	ICCD	ICCD
Lens	Nikon - Nikkor	B. Halle Nacht - U.V.
Lens features	50 mm - f /1.8	100 mm - f /4 U.V. glass
Pixel/mm	4.72	6.12
Image size [pix]	512 x 512	512 x 512
Image size [mm]	108x108	83x83
Gating time [μs]	20	20
Test repetitions	5	5
Filtering [nm]	430 ± 5	310 ± 5
Intensifier gain	Maximum	Max. at the ignition and reduced when the flame gets brighter

Figure 2

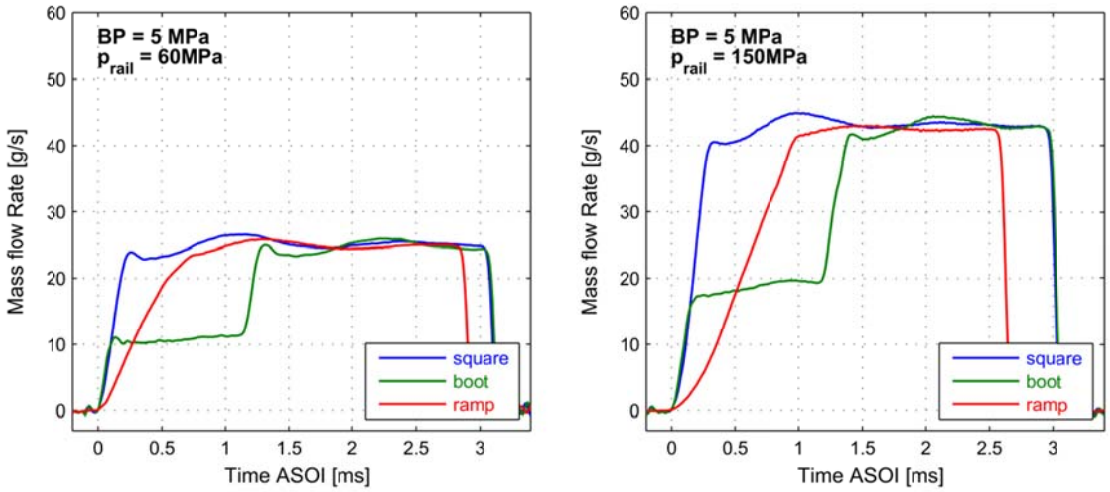

Figure 3

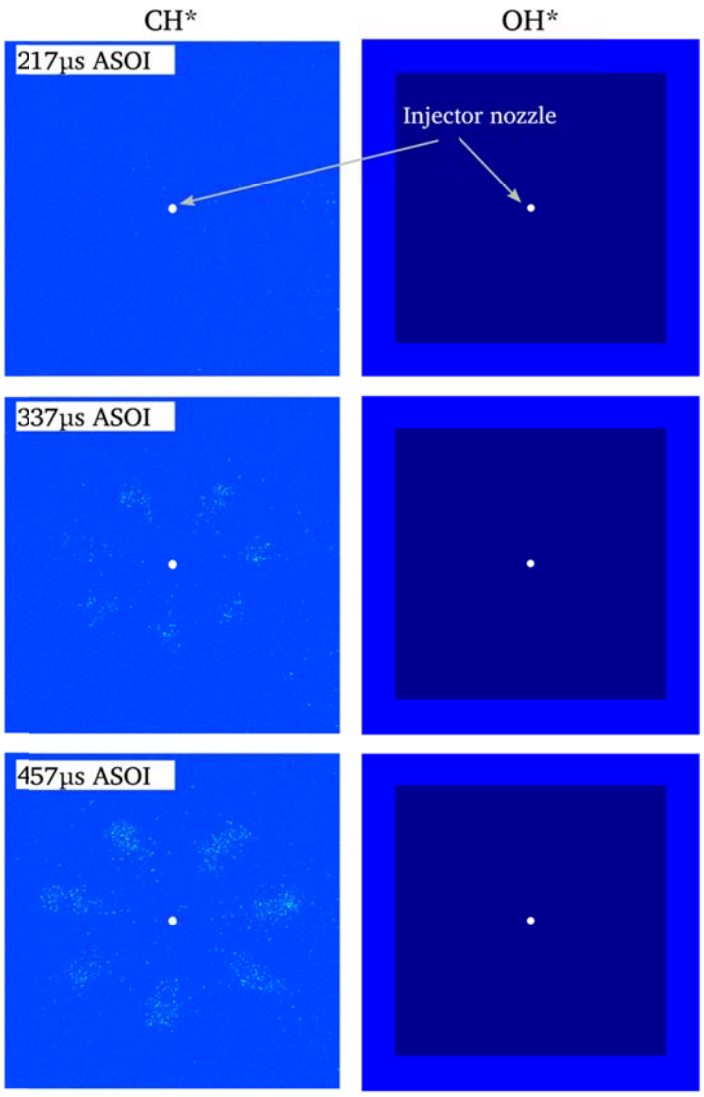

Figure 4

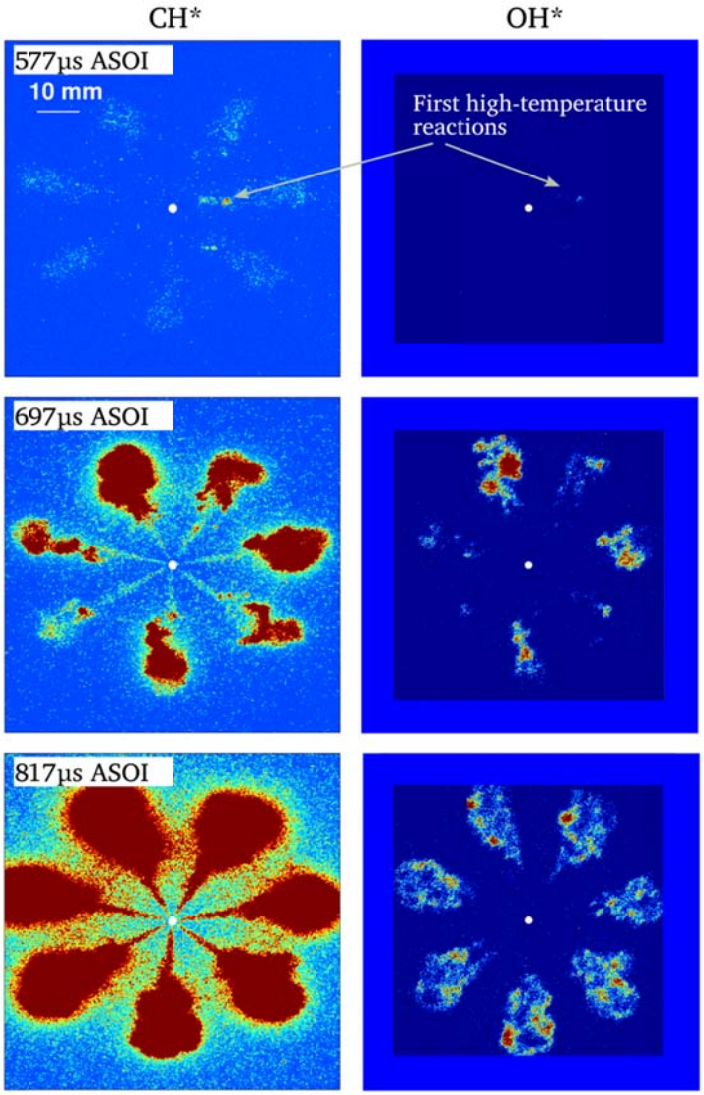

Figure 5

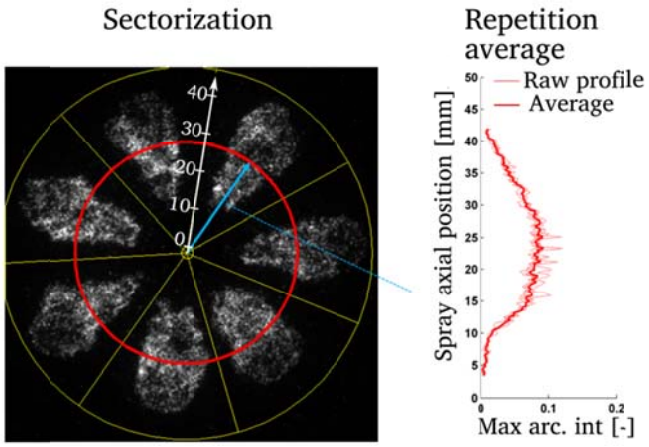

Figure 6

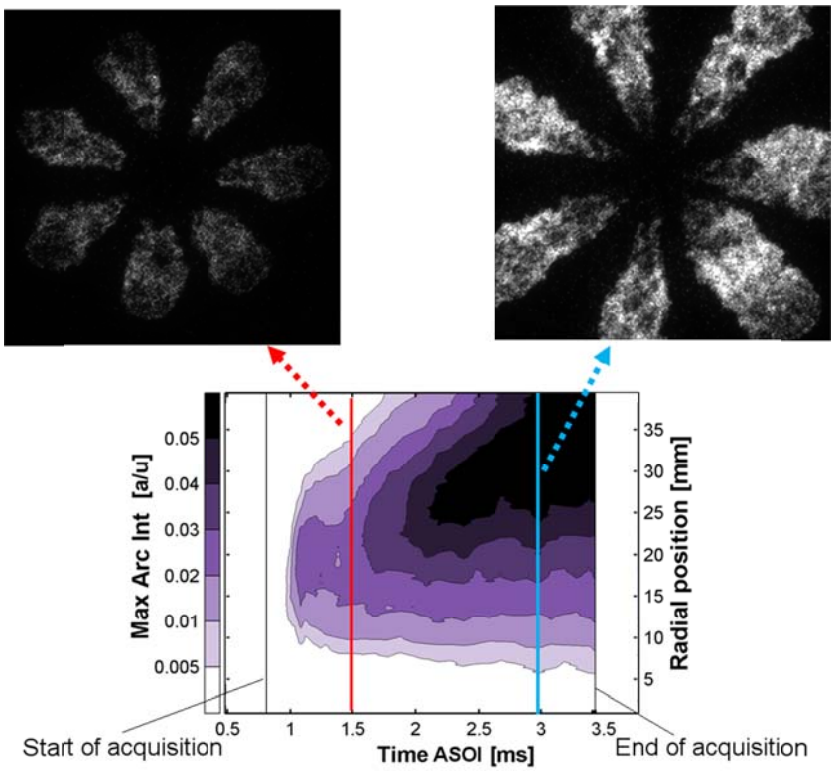

Figure 7

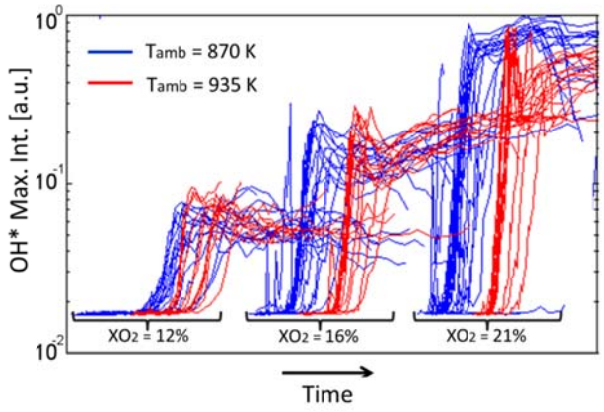

Figure 8

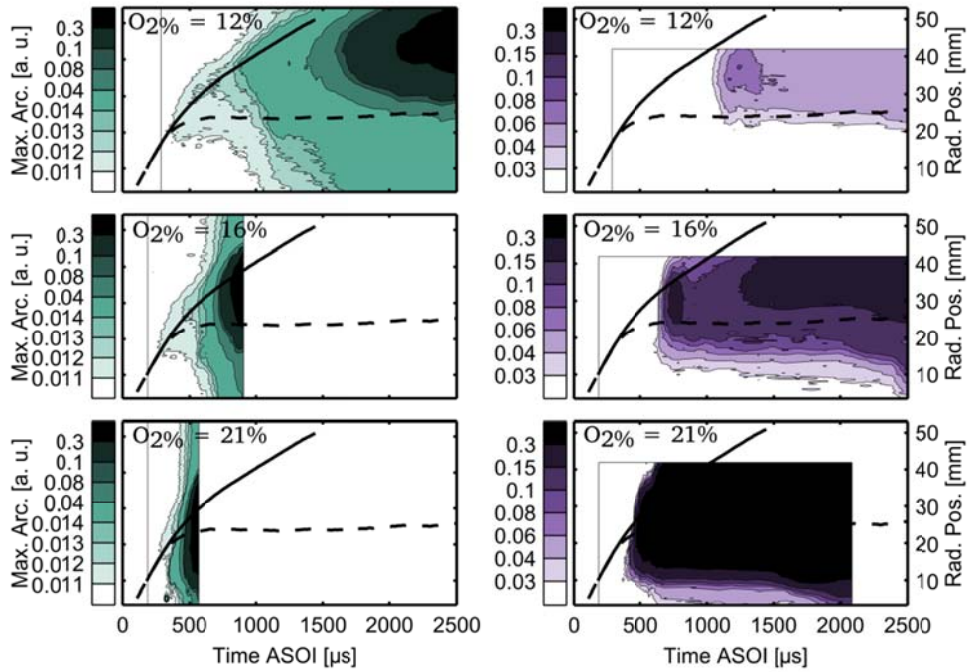

Figure 9

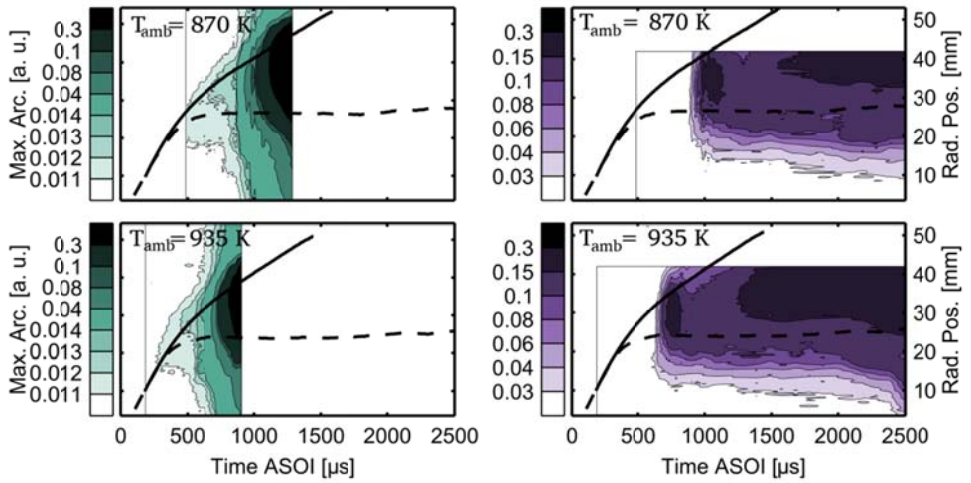

Figure 10

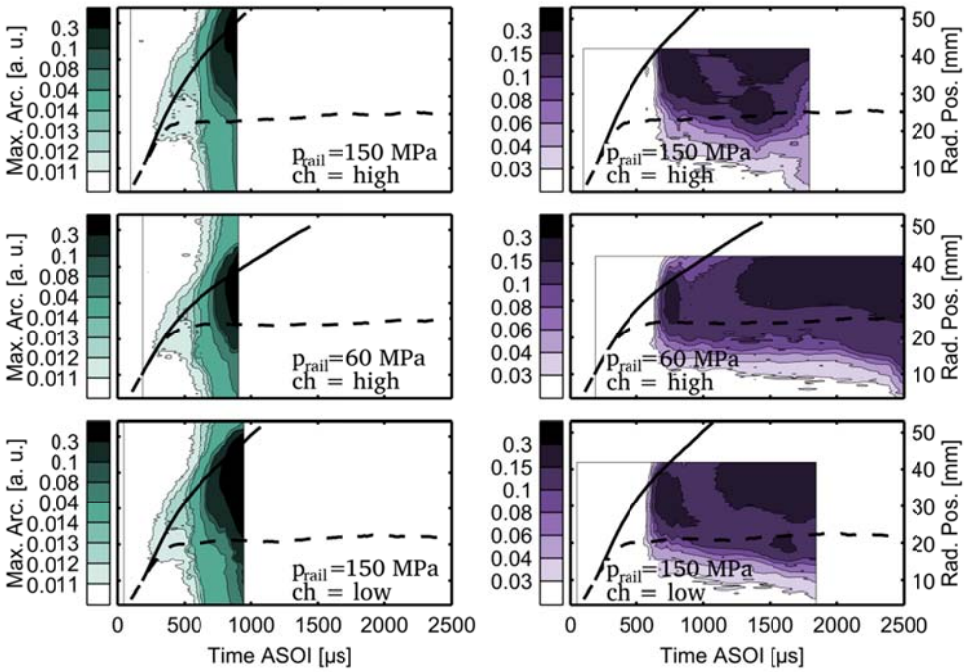

Figure 11

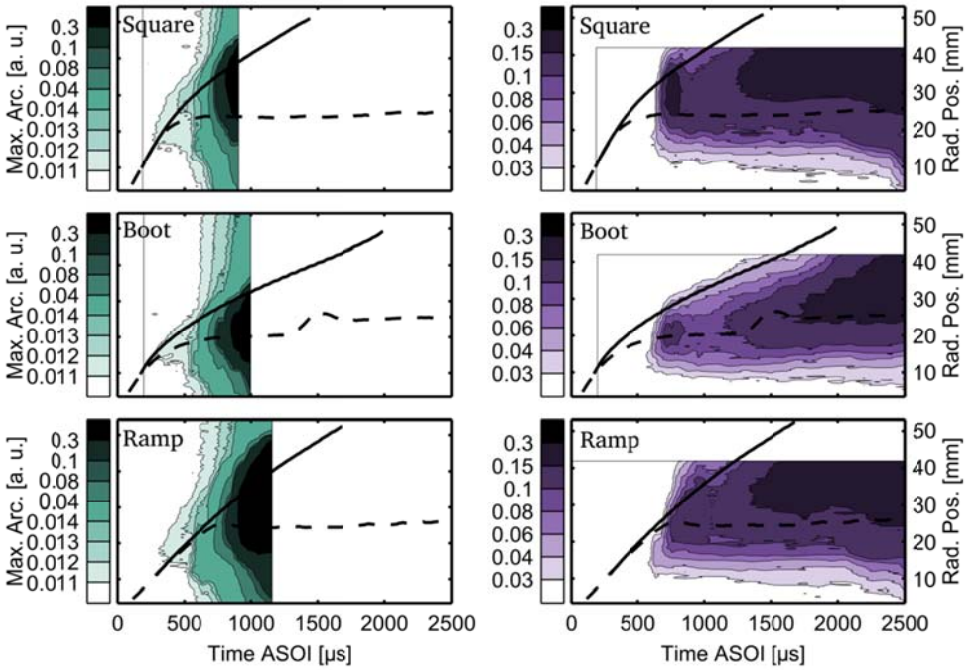

Figure 12

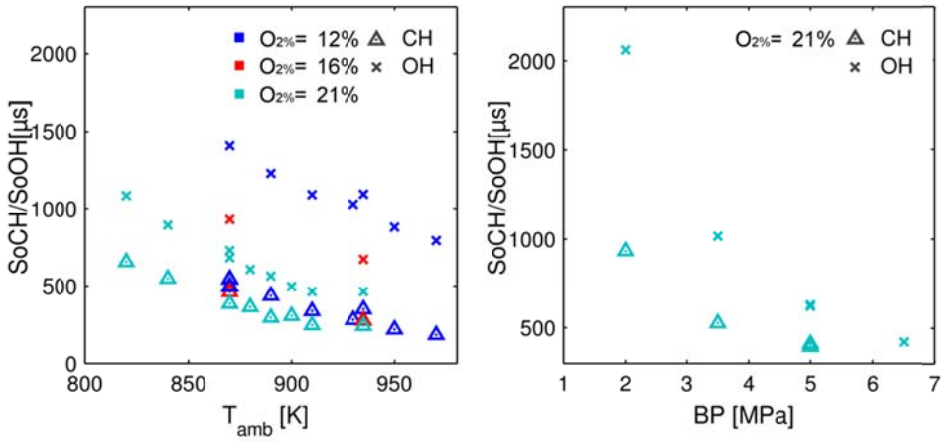

Figure 13

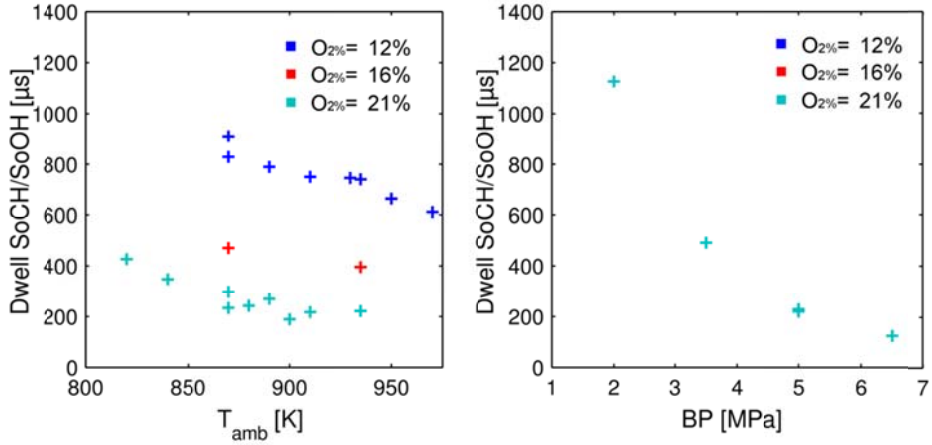

Figure 14

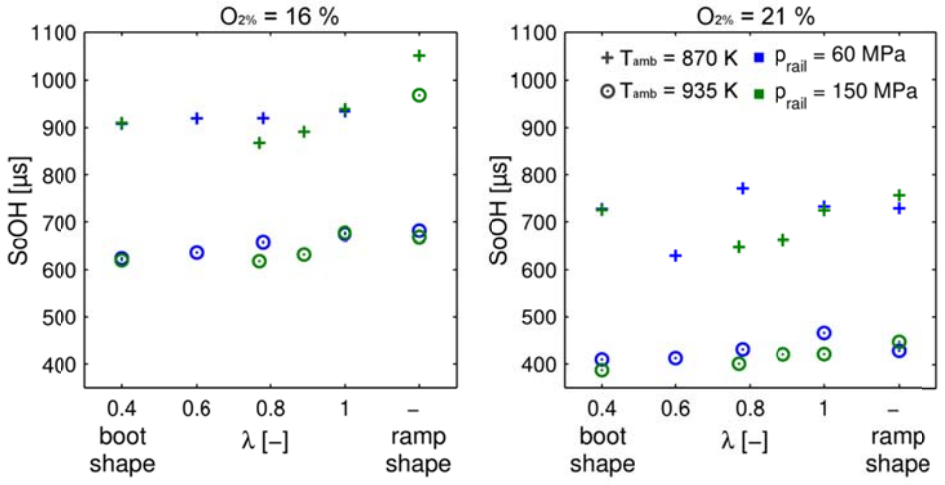

Figure 15

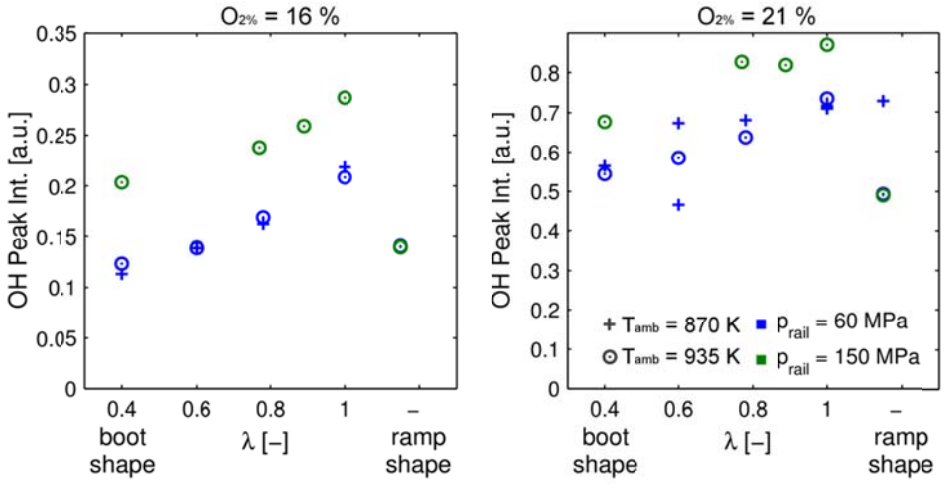

Figure 16

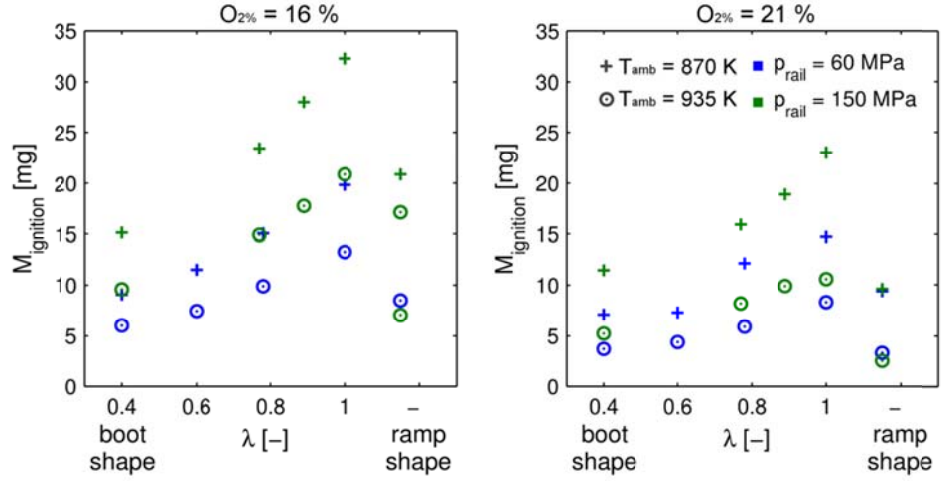

Figure 17

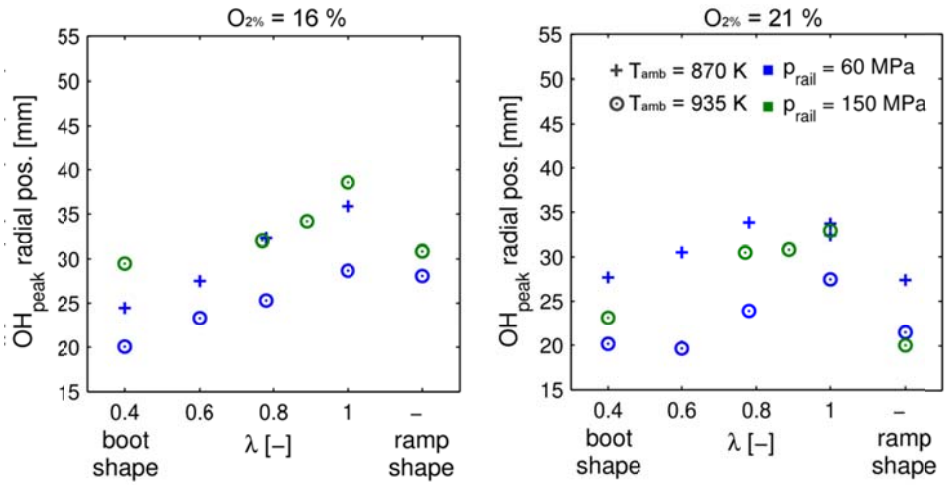

Figure 18

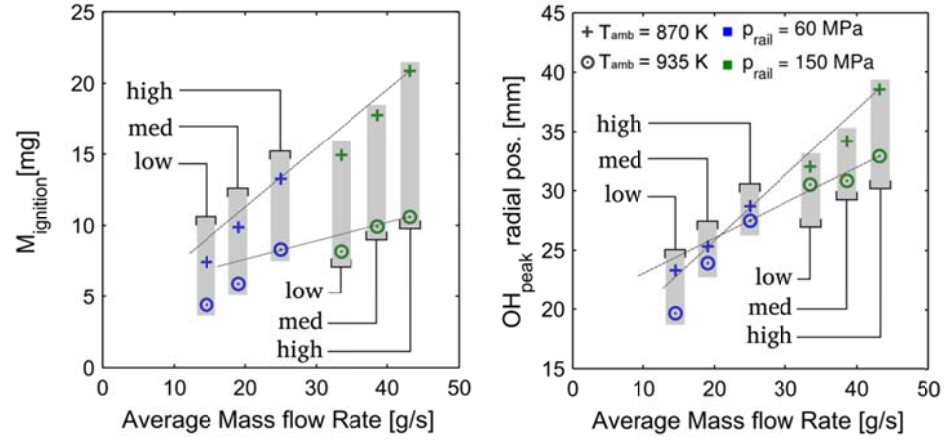

Figure 19